3.4 Pion absorption from the lowest atomic orbital

3.4.1 Pion absorption in ^{2}H

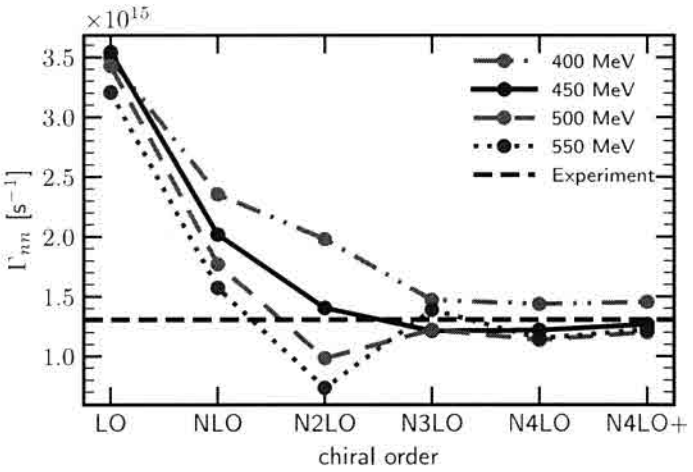

Figure 3.48: Absorption rate for the reaction $\pi^- + {}^2\mathrm{H} \to n + n$. The rates were calculated using the SMS force with different chiral orders and cut-off values. The results were obtained using the single-nucleon transition operator and including two-nucleon contributions at the leading order. The figure shows the results obtained using the plane wave (PW) plus two-neutron rescattering (Full) parts. The experimental value is extracted from the hadronic ground-state broadening in pionic deuterium and taken from Ref. [85, 86].

In Fig. 3.48 the absorption rate Γ_{nn} is shown for the process $\pi^- + {}^2\mathrm{H} \to n + n$ as a dependance on the chiral order (horizontal axis) and cutoff parameter (different lines) as well as experimental data extracted from [85, 86]. We see the noticeable difference between predictions obtained using different Λ. The impact of chiral orders is large at LO and NLO and is gradually decreasing, and N^{3}LO-N^{4}LO-N^{4}LO$^+$ steps are almost invisible. The comparison with experimental data shows that our predications converge to a correct value coming closely to it all large chiral orders.

3.4.2 Pion absorption in ^{3}He

In Fig. 3.49 and 3.50 the pion absorption rates are presented as a function of the chiral order and for different values of the cut-off parameter for $\pi^- + {}^3\mathrm{He} \to p + n + n$ and $\pi^- + {}^3\mathrm{He} \to n + d$ reactions, respectively. Both figures show that with fixed chiral order the arrangement of absorption rates obtained with various values of the cut-off parameter remains the same, namely with increasing Λ, absorption rate decreases. The only exception in both cases appears at N^{3}LO where prediction with $\Lambda = 550\,\mathrm{MeV}$ goes above other predictions. At the next order, N^{4}LO, it comes back to the normal arrangement. This behavior may be connected to the ^{3}He wave function resulting from the 3NF used for the calculation. In order to check that I show in Fig. 3.51 a corresponding figure for a ^{3}He proton radius r_p calculated with and without 3NF (left and right panels, respectively). Results obtained with the 3NF show similar deviation at N^{3}LO while radious obtained without the 3NF does not. Nevertheless, the spread of predictions with

respect to the cut-off values seen in Fig. 3.51 is much smaller with the 3NF and deviation seems to be not crucial as total difference between predictions in this case is very small.

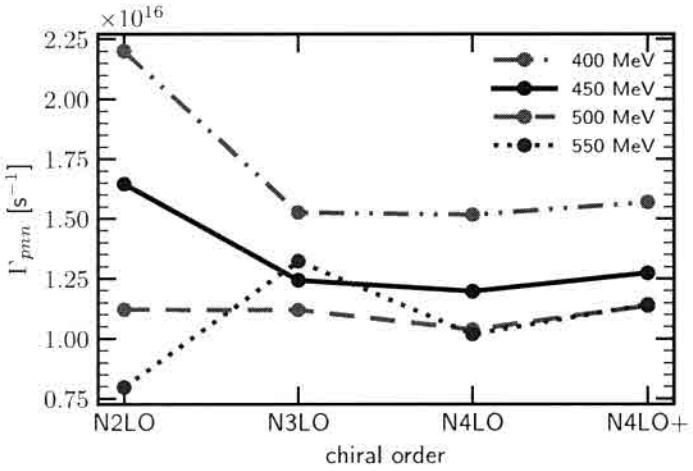

Figure 3.49: Absorption rate for $\pi^- + {}^3\mathrm{He} \to p+n+n$ reaction as a function of the chiral order and with different values of the cut-off parameter Λ. Predictions were obtained with the SMS NN interaction at given order combined with N^{2}LO 3NF.

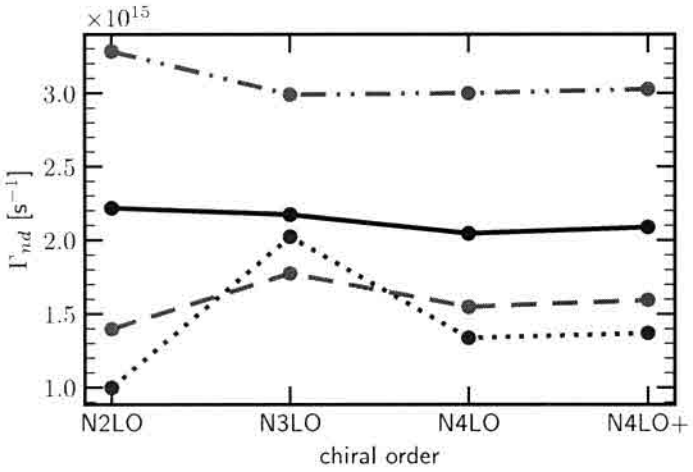

Figure 3.50: The same as in Fig. 3.49, but for $\pi^- + {}^3\mathrm{He} \to n + d$ reaction.

By its nature the total absorption rates cannot deliver details on distribution of contributions arising from various dynamical ingredients to the absorption process in the phase-space. Thus in following I show various intensity plots revealing phase-space regions of special interest.

Let us remind that in case of absorption rates only two kinetical variables are neccessary to define exclusive kinematical configuration. *That is, because for that process there is full rotational symmetry, as none of vectors define the $\mathcal{S}$-axis.*

In Figs. 3.52 and 3.53 I show intensity plots for the double differential absorption rates $d^2\Gamma_{pmn}/dE_1dE_2$ for the $\pi^- + {}^3\mathrm{He} \to p+n+n$ process as functions of the nucleons energies (assuming nucleon number 1 to be proton) and of Dalitz coordinates (x and y), respectively.

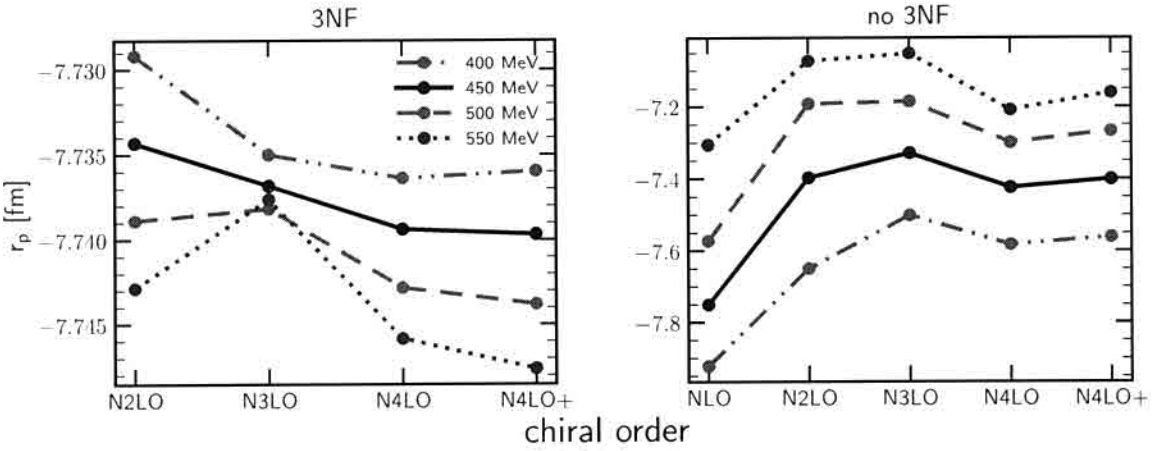

Figure 3.51: *check mt3* Proton radius r_p as a function of the chiral order calculated with different values of the cut-off parameter Λ. The radius was calculated with 2NF and 3NF (left panel) ~~and~~ with 2NF only (right panel).

The coordinates x and y are defined as:

$$x = 3(E_1 + 2E_2 - E)/E,$$
$$y = (3E_1 - E)/E, \tag{3.3}$$

where E is a total kinetic 3N energy. These coordinates are restricted to the region where $r^2 \equiv x^2 + y^2 \leq 1$.

Each of two figures consists of four panels representing predictions obtained with different values of the cut-off parameter Λ. The difference between predictions which can be immediately noticed with the naked eye - is that area of the central region (corresponding to smallest ~~values~~) becomes larger with increasing Λ. It coheres to what we saw in Fig. 3.49 where total absorption rate was inversely correlated with cut-off parameter. The dominant contribution comes from the region with lowest proton energy values of $E_1 \to 0$ where both neutrons have similar large values. This is a situation when proton is a spectator ~~while~~ both neutrons share all energy - quasi-free scattering(QFS).

Another region with high absorption rate is neutron-neutron final state interaction (FSI(nn)). It is located at high E_1 when proton gets one third part of total energy while neutrons both get one sixth.

Next I show similar ~~colormaps~~ but for the predictions obtained with plane wave component only (without rescattering part), in Figs. 3.54 and 3.55. ~~Presented plots show~~ that the difference of predictions obtained without rescattering part with ~~full~~ is very large. Predicted values are few times larger and the distribution is completely different. The FSI(nn) region is not presented here in a sense that there is no peak with respect to other ~~values~~. The QFS region is, on the contrary, ~~which~~ obviously tells us that one has to take into account rescattering part in order to obtain ~~relevant results~~.

Results obtained with Plane wave plus rescattering part ~~and~~ with single nucleon current only are presented in Figs. 3.56 and 3.57. As previously, each panel in figures presents predictions obtained with different values of the cut-off parameter Λ. In contrast to the ~~configurations~~ shown above, the change of the cut-off value has larger impact here: we

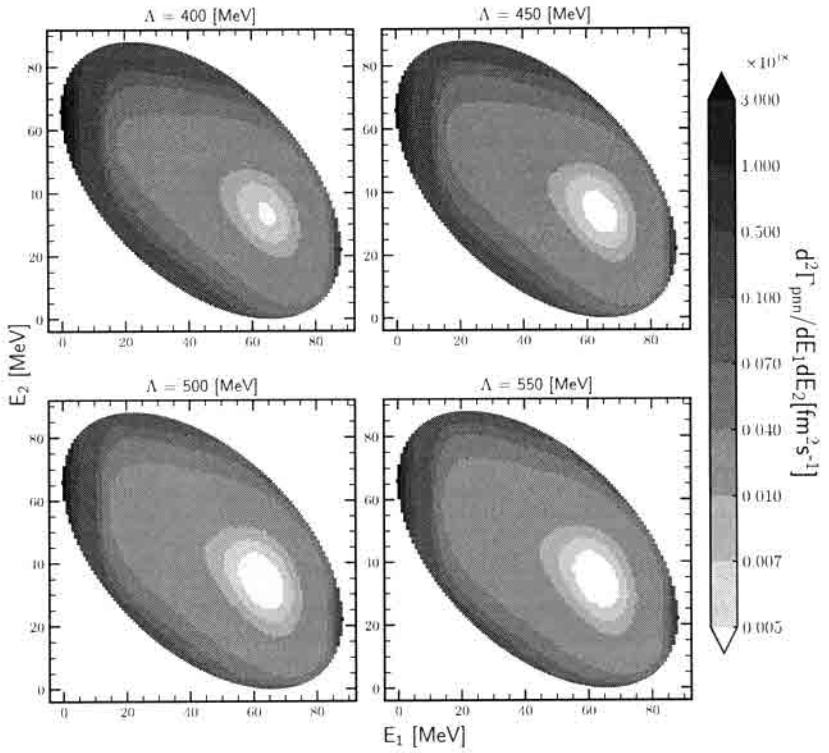

Figure 3.52: Intensity plots for the double differential absorption rates $d^2\Gamma_{pnn}/dE_1dE_2$ for the $\pi^- + {}^3\mathrm{He} \to p + n + n$ process, obtained using the SMS potential at $\mathrm{N^4LO^+}$ with all contributions possible: plane wave − rescattering, 1NC − 2N, 2NF−3NF. Each panel present predictions obtained with different values of the cut-off parameter Λ: from 400 MeV (upper left) to 550 MeV (lower right). Nucleon 1 is a proton.

see that there is a different pattern in each panel. It does not change dramatically, but two peaks inside the figure become more or less clear. On the other hand, the distribution of the absorption rate is very different from the one, obtained with more complete components setup (Figs. 3.52 and 3.53).

Figs. 3.58 and 3.59 show prediction obtained using similar configuration as in Figs. 3.52 and 3.53, but each panel includes predictions obtained with different chiral orders of the SMS potential. We see that predictions are not sensitive to the chiral order and even $\mathrm{N^2LO}$ predictions are pretty much similar to ones obtained with the most advanced $\mathrm{N^4LO}$ potential.

Following figures demonstrate the same results but from the different prospective. Namely in Fig. 3.60 I show differential absorption rate $d\Gamma_{pnn}/dE_p$ that is the same as in e.g. Fig. 3.58, but integrated over E_n. All the results are obtained with the most advanced setup (plane wave − rescattering, 1NC − 2N, 2NF−3NF). The left panel consists of the results with $\Lambda = 450$ MeV and each curve correspond to a particular chiral order. Interesting region here is a maximum point, which corresponds to a bottom part of the circles from Fig. 3.58. At the point of maximum $\mathrm{N^2LO}$ outstands from other results as its point of maximum is noticeably higher. At $E_p = 0.92$ MeV (maximum point) the value of $\mathrm{N^2LO}$ is 1.37 times larger than one from $\mathrm{N^4LO^+}$ (3.44×10^{17} fm s^{-1} vs 2.52×10^{17} fm s^{-1}) - the relative difference is 31.1 %. At the same time, the relative difference between all the predictions except for $\mathrm{N^2LO}$ is 8.3 %.